Electric-field-induced superconductivity in an insulator

K. UENO[1]*, S. NAKAMURA[2], H. SHIMOTANI[3], A. OHTOMO[3], N. KIMURA[2], T. NOJIMA[2], H. AOKI[2], Y. IWASA[3,4] AND M. KAWASAKI[1,3,4]*

[1] WPI-Advanced Institute for Materials Research, Tohoku University, Sendai 980-8577, Japan
[2] Center for Low Temperature Science, Tohoku University, Sendai 980-8577, Japan
[3] Institute for Materials Research, Tohoku University, Sendai 980-8577, Japan
[4] CREST, Japan Science and Technology Agency, Tokyo 102-0075, Japan
*e-mail: uenok@imr.tohoku.ac.jp; kawasaki@imr.tohoku.ac.jp

Electric field control of charge carrier density has long been a key technology to tune the physical properties of condensed matter, exploring the modern semiconductor industry. One of the big challenges is to increase the maximum attainable carrier density so that we can induce superconductivity in field-effect-transistor geometry. However, such experiments have so far been limited to modulation of the critical temperature in originally conducting samples because of dielectric breakdown[1–4]. Here we report electric-field-induced superconductivity in an insulator by using an electric-double-layer gating in an organic electrolyte[5]. Sheet carrier density was enhanced from zero to 10^{14} cm^{-2} by applying a gate voltage of up to 3.5 V to a pristine SrTiO$_3$ single-crystal channel. A two-dimensional superconducting state emerged below a critical temperature of 0.4 K, comparable to the maximum value for chemically doped bulk crystals[6], indicating this method as promising for searching for unprecedented superconducting states.

Carrier density is a key parameter of the electronic state of condensed matter. Substitutional or interstitial chemical doping is the most common method used to change the carrier density, but the structural disorder inherent in this method always causes unnecessary complexity in the physical properties. On the other hand, electric-field tuning of surface carrier density through carrier accumulation or depletion in metal–insulator–semiconductor field-effect-transistor (FET) structures is free from this sort of structural disorder, and thus is attracting growing interest as a new method to control properties of materials such as ferromagnetic semiconductors and oxide superconductors[1,2,7]. Electric-field-induced superconductivity has been the subject of long-standing focus since the 1960s (ref. 8), and various materials have been tested. Among them, SrTiO$_3$ is a promising target material for this purpose, because it is known to show bulk superconductivity with a relatively low carrier density when chemically doped[6]. Nevertheless, the typical sheet carrier density, n_{2D}, attainable in conventional metal–insulator–semiconductor FET structures is only $\sim 1 \times 10^{13}$ cm^{-2}, which is still unsatisfactory for inducing superconductivity, though insulator-to-metal transition has been demonstrated in an undoped SrTiO$_3$ channel[9–12]. The use of ferroelectric gate structures enables switching of the critical temperature, T_c, from 0.24 to 0.3 K in chemically doped conducting SrTiO$_3$ (refs 3,4). However, there

have been no reports on superconductivity induced purely by an electric-field effect in a completely insulating material without the aid of chemical doping.

To overcome this limitation, we have used a different type of FET, based on an electrochemical concept. When a voltage is applied across two electrodes in an electrochemical cell, solvated ions in the electrolyte move towards both electrodes according to their charge polarity. As a result, the ions are collected on the electrode surface to form an electric double layer that effectively works as a subnanometre-gap capacitor with solvating polymer molecules as a dielectric layer. On the electrode side, opposite charges of equivalent density accumulate[5]. If one of the electrodes is replaced by a semiconductor with source and drain electrodes, the system works as a FET. We call this device an electric-double-layer transistor. Using this device, an accumulation of extremely high carrier densities up to 10^{15} cm^{-2} (refs 13,14) and insulator-to-metal transitions have been demonstrated for organic polymers, InO$_x$ polycrystalline films and ZnO single-crystal films[13–16].

In this study, electrons were accumulated at a pristine SrTiO$_3$ single-crystal surface with an electric-double-layer-transistor configuration, as shown in Fig. 1a. We fabricated Hall-bar devices on atomically flat (100) surfaces of SrTiO$_3$ single crystals[17] and measured the four-terminal sheet resistance, R_s, and Hall coefficient, R_H, of the channels (see Fig. 1b and Fig. 1c, inset). The wired specimen and a Pt gate electrode were immersed in a polymer electrolyte, polyethylene oxide, containing KClO$_4$ ([K]:[O] in polyethylene oxide = 1:100) as an electrolyte salt.

Figure 1c shows a transfer curve (gate voltage V_G versus drain current I_D) measured at a drain voltage V_D of -0.5 V and a temperature of 300 K. We observed an abrupt increase in I_D at $V_G > 1$ V, which in turn yielded an on–off ratio greater than 10^3 towards $V_G = 3$ V, clearly demonstrating n-type FET action. The off-state I_D was less than 1 nA, indicating that the channel was fairly insulating (>1 GΩ). The gate leakage current I_G, presumably induced by the electrochemical decomposition of impurity water in electrolyte, was kept lower than 10 nA in the entire V_G range. Figure 1d shows I_D–V_D curves obtained in a V_G range of 1.5–3.0 V; these also reflect n-type FET characteristics. Temperature dependencies of R_s and R_H are summarized in Fig. 2. They were measured while the sample was cooled from 300 to 2 K with a certain gate bias, because motion of ions in the electrolyte is

855
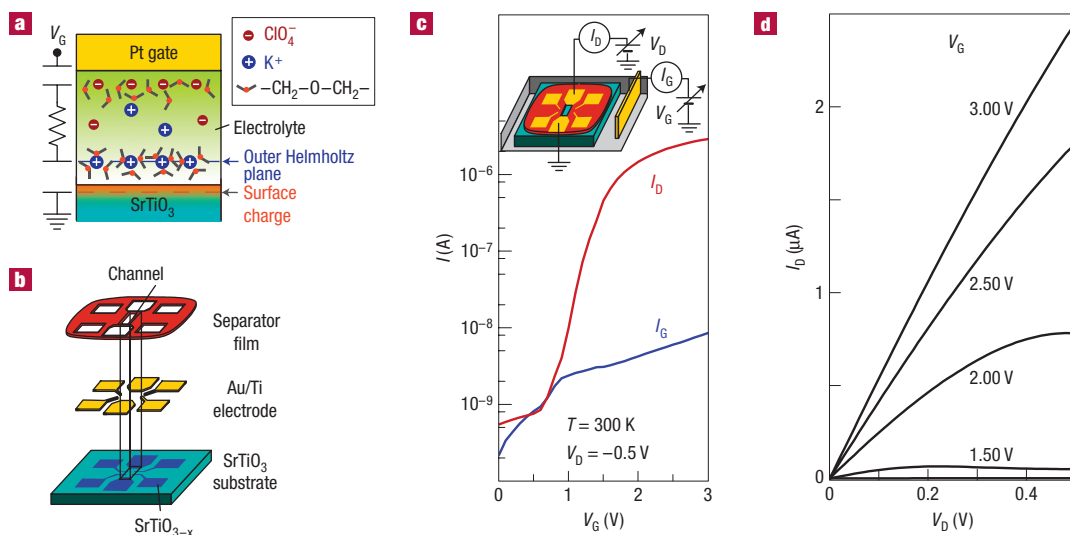
Figure 1 Schematic structures and current–voltage characteristics of an electric-double-layer field-effect transistor. a, Schematic diagram of an electric double layer formed at an electrolyte–SrTiO$_3$ interface. Cations (K$^+$) in the electrolyte are solvated by polyethylene oxide molecules and are electrostatically adsorbed on the SrTiO$_3$ surface on application of a positive gate bias to the Pt electrode, forming an outer Helmholtz plane with positive charge. A negative image charge is induced in the SrTiO$_3$ surface layer, forming an electric-double-layer capacitor with a sheet of the solvating molecules (about 1 nm thick) as a dielectric layer. We used a polyethylene oxide with a molecular weight of 1,000 and melting point of 310 K. **b,** Schematic diagram of device structure with a Hall-bar geometry. The blue regions of the SrTiO$_3$ surface were metallized by ion milling (acceleration voltage of 350 V, approximately 100 nm thick) and covered by Ti (100 nm) and Au (100 nm) layers to form contact pads and lead lines[12]. An insulating separator layer with openings for the SrTiO$_3$ channel (15 μm × 200 μm) was prepared with a hard-baked photoresist (1 μm thick), which prevents contact between the SrTiO$_3$ and the electrolyte. The distance between the voltage probes is 30 μm. We confirmed that the metallized SrTiO$_3$ surface was metallic but not superconducting down to 0.02 K. **c,** Drain current I_D versus gate voltage V_G transfer curve (red) measured at a drain voltage V_D of −0.5 V and at a V_G sweep rate of 0.05 mV s^{-1}. In this quasi-static mode, hysteresis was negligibly small. Also shown is the leakage current I_G (blue), which becomes negligible below 280 K owing to freeze-out of the mobile ions. The inset shows the source–drain–gate contact configuration with an earthed source. **d,** I_D–V_D curves measured at 300 K with various values of V_G.

too slow for active measurement at low temperature. Metallic states emerged for $V_G \geqslant 2.5$ V, showing reduction in R_s by almost two orders of magnitude. This is in striking contrast to the insulating behaviour for $V_G \leqslant 2.25$ V, where non-degenerate electrons rapidly freeze with decreasing temperature.

To rule out electrochemical reactions as an origin of donated metallic conduction, we characterized the SrTiO$_3$ surface, after removing the electrolyte, by using atomic force microscopy and secondary ion mass spectroscopy depth profiling. The atomic force microscopy image of the channel region after repeated FET experiments showed a well-defined structure with 0.4 nm steps and flat terraces, similar to the original structure (see Supplementary Information, Fig. S1a,b). The signal intensity of potassium was close to the detection limit, and there was no appreciable difference between the original and voltage-stressed surfaces (see Supplementary Information, Fig. S1c,d). Therefore, the intercalation of K$^+$ acting as a donor is not likely to occur. Formation of oxygen vacancies may be one possible explanation. However, we observed fairly rapid decrease in I_D when V_G was changed stepwise from 3.5 to 0 V (see Supplementary Information, Fig. S1e). If oxygen vacancies were the origin of the channel conduction, slow oxygen diffusion might enable a rapid increase in I_D but would not give a rapid decrease in I_D because deeper regions would be kept conducting by the remaining oxygen vacancies.

Figure 2b shows the temperature dependence of the Hall mobility, μ_H, and n_{2D} ($= -1/R_H e$) for various values of V_G. The temperature dependence of μ_H was almost identical regardless of V_G, whereas μ_H steeply increased as the temperature was lowered to reach 500–1,000 cm^2 V^{-1} s^{-1}. Both temperature and carrier-density dependencies of μ_H are similar to those for chemically doped
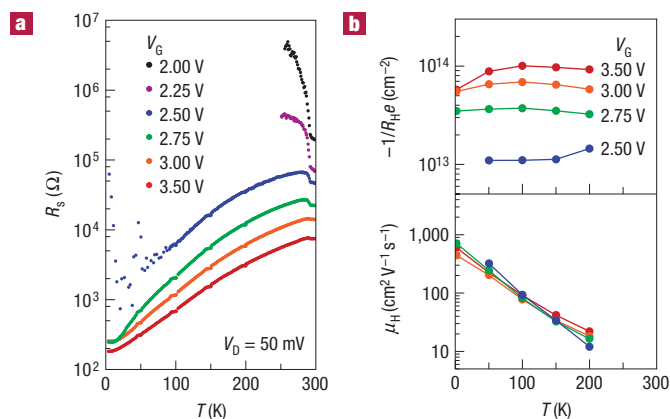
Figure 2 Electrical properties of accumulated SrTiO$_3$ surface layer.
a, Temperature dependence of channel sheet resistance R_s measured while applying various gate voltages V_G. The discontinuous change in R_s at 280 K is an artefact arising from virtually suppressed I_G below that temperature. **b,** The upper and lower panels respectively show the temperature dependence of the sheet carrier density, $n_{2D} = -1/R_H e$, and mobility, μ_H, evaluated by Hall effect measurements.

metallic or superconducting SrTiO$_3$ bulk crystals[6,18]. Virtually independent of temperature, n_{2D} increased almost linearly with V_G above a threshold of about 2.3 V. When V_G was 3.5 V, n_{2D} exceeded 1×10^{14} cm^{-2}, which is far above the maximum value induced in conventional metal–insulator–semiconductor
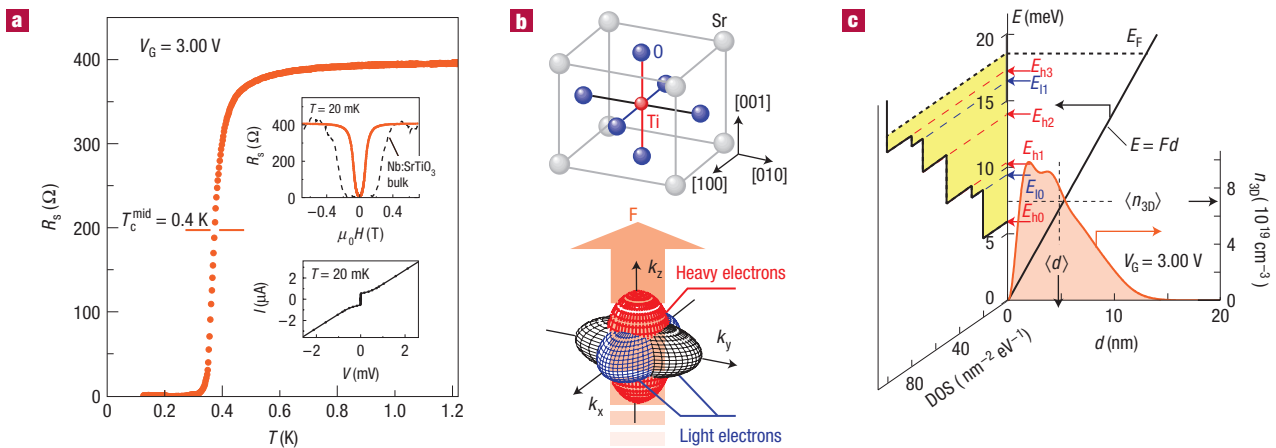
Figure 3 Superconducting properties and electronic structure of the SrTiO$_3$ channel under a gate bias voltage $V_G = 3$ V. a, Temperature dependence of R_s. The dashed line denotes the mid-point of the transition. The upper inset shows the magnetic-field ($\mu_0 H$) dependence of R_s at 0.02 K. A normalized R–H curve for a SrTi$_{0.998}$Nb$_{0.002}$O$_3$ bulk single crystal is also plotted as the dotted line for comparison. The lower inset shows the I–V curve at 0.02 K. **b**, A schematic diagram of the crystal structure and constant-energy surfaces of three conduction-band valleys of SrTiO$_3$. The red arrow denotes the direction of a confinement electric field F. **c**, Right panel: Depth profile of the volume carrier density n_{3D} (red) and potential E (black) under a triangular-potential approximation. $\langle d \rangle$ and E_F denote the mean depth of the carrier distribution and the Fermi energy, respectively. Left panel: Density of states (DOS) as a function of energy E. Here, E_{hn} and E_{ln} denote the nth subband energies for the heavy (h) and light (l) electrons, respectively.

FETs ($\sim 1 \times 10^{13}$ cm^{-2}). The linear n_{2D}–V_G dependence gives an electric-double-layer capacitance of 13 µF cm^{-2}, which is in good agreement with that obtained from a capacitance measurement in LiClO$_4$–polyethylene oxide electrolyte, and corresponds to a parallel-plate capacitor with a thickness of 0.6 nm and relative dielectric constant of 10 as a solvating polymer dielectric layer[19]. We note that the n_{2D} range in the metallic state is much smaller than the previously reported ones at LaAlO$_3$–SrTiO$_3$ interfaces that show oscillating magnetoresistance[20] ($\sim 1 \times 10^{17}$ cm^{-2}), but is similar to the ones at interfaces reported to be magnetic[21] ($\sim 1 \times 10^{14}$ cm^{-2}) and superconducting[22] ($\sim 4 \times 10^{13}$ cm^{-2}) (see Supplementary Information, Fig. S2).

Now we present the data measured at temperatures below 2 K in a dilution refrigerator. Figure 3 shows the temperature dependence of R_s at $V_G = 3$ V, where a sharp superconducting transition is clearly seen, with a mid-point critical temperature $T_c^{mid} = 0.4$ K, where $R_s(T_c^{mid}) = 0.5 \times R_s (1$ K$)$, and a zero-resistance temperature $T_c^{zero} = 0.28$ K. When we applied a magnetic field $\mu_0 H$ perpendicular to the sample surface at 0.02 K, R_s recovered its normal-state value (0.4 kΩ) above 0.2 T (upper inset). The I_D–V_D curve in zero field indicated a supercurrent lasting up to 0.5 µA (lower inset). These results demonstrate the electric-field-induced superconductivity in SrTiO$_3$. It is noted that the shape of the R–H curve is different from that obtained for a SrTi$_{0.998}$Nb$_{0.002}$O$_3$ (Nb:SrTiO$_3$) bulk single crystal with a T_c^{mid} of 0.4 K and a volume carrier density of 3.3×10^{19} cm^{-3}. The upper critical field H_c, where $R(H_c) = 0.5R(0$ T$)$, was 0.08 T for the electric-double-layer transistor, which is about one-third of H_c for Nb:SrTiO$_3$ (0.2 T).

We compared our data with those reported for chemically doped bulk samples. To estimate the volume carrier density n_{3D} for our device, we deduced the two-dimensional subband structure and the depth profile of n_{3D} (see details in Supplementary Information). The accumulation layer was assumed to be a quantum well with a triangular potential along the [001] direction[23]. Taking into account the electric-field dependence of the dielectric constant obtained in bulk material[24], the confinement electric field F was deduced to be 14 kV cm^{-1} for

$n_{2D} = 5 \times 10^{13}$ cm^{-2} at $V_G = 3$ V. We also consider the conduction band of SrTiO$_3$ composed of three doubly degenerate valleys centred at the Γ point with their long axes along {100}, as shown in Fig. 3b (ref. 25), and with longitudinal (m_l^*) and transverse (m_t^*) effective masses of $4.8m_0$ and $1.2m_0$, respectively, where m_0 is the free-electron mass[26–28]. Due to the anisotropic effective mass, one valley along the [001] direction (heavy electrons) has heavier effective mass for the motion along the confinement direction compared with the other two valleys (light electrons), resulting in lower subband energies. The left panel of Fig. 3c shows subband energies of the quantum well. The fourth and second subbands are partially occupied for the heavy and light electrons, respectively. Therefore, scattering between subbands can occur, indicating that this system is not truly two dimensional but rather three dimensional in the normal state. The right-hand panel of Fig. 3c shows the depth profile of n_{3D} as a function of depth d deduced by taking into account the population of occupied subbands (see equation (7) in Supplementary Information). As can be seen, most of the accumulated carriers were confined within 10 nm of the surface, and the weighted mean values of carrier distribution depth, $\langle d \rangle$, and volume carrier density, $\langle n_{3D} \rangle$, were calculated to be 5 nm and 7.0×10^{19} cm^{-3}, respectively, from equations (8) and (9) in Supplementary Information. The latter value is similar to the carrier density of chemically doped SrTiO$_3$, which has a maximum T_c^{mid} of 0.5 K (ref. 6).

Superconducting transitions were characterized for various values of V_G, as shown in Fig. 4a. A steep decrease in R_s was observed at around 0.4 K for all values of V_G. The mid-point critical temperature T_c^{mid} was almost constant at 0.4 K regardless of the large variation in n_{2D} (1–10×10^{13} cm^{-2}), as shown in the top panel of Fig. 4b. In addition, H_c was virtually independent of V_G (0.08–0.1 T, not shown). These V_G-independent critical parameters are quite different from those observed for chemically doped SrTiO$_3$ crystals, where T_c appreciably depends on carrier density[6]. The coherence length of 51–57 nm deduced from H_c is far greater than the carrier distribution depth ($\langle d \rangle = 5$–15 nm), indicating that the superconductivity is two dimensional.
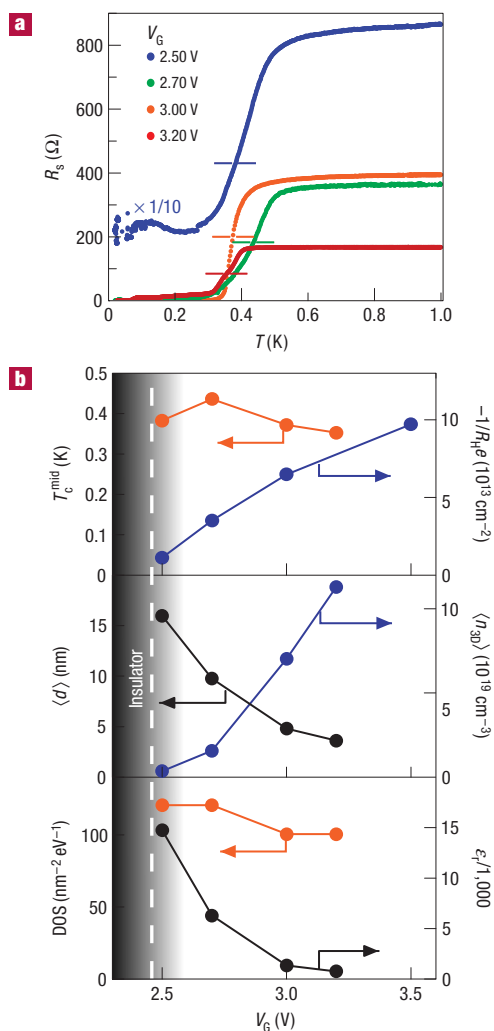
Figure 4 Gate voltage, V_G, dependence of transport properties and electronic parameters deduced with the triangular-potential approximation.
a, Temperature dependence of R_s. Dashed lines denote the mid-point of the transition. **b**, Top panel: Mid-point critical temperature, T_c^{mid}, and sheet carrier density, $n_{2D} = -1/R_H e$, at 150 K. Middle and bottom panels: Mean depth of carrier distribution, $\langle d \rangle$, mean volume carrier density, $\langle n_{3D} \rangle$, density of states at the Fermi energy, DOS, and dielectric constant, ε_r, in the accumulation layer.

As a final remark, we discuss the carrier density dependence of the electronic states in the accumulation layer of $SrTiO_3$. The middle panel of Fig. 4b shows $\langle d \rangle$ and $\langle n_{3D} \rangle$ as functions of V_G. At $V_G = 2.5$ V, the large dielectric constant of $SrTiO_3$ weakened the confinement potential, resulting in a spreading accumulation layer ($\langle d \rangle = 16$ nm) and a decrease in $\langle n_{3D} \rangle$ (3×10^{18} cm^{-3}), where superconductivity is expected to vanish in chemically doped $SrTiO_3$ (ref. 6). The reason for this apparently higher T_c in the low-$\langle n_{3D} \rangle$ channel than in the bulk (see also Supplementary Information, Fig. S3c) needs further study to be addressed. In the following, a possible relevance for constant T_c is proposed as the constant density of states (DOS) at Fermi energy (E_F). An increase of V_G reduced the dielectric constant of $SrTiO_3$ owing to its incipient ferroelectricity and greatly enhanced the carrier confinement. As a result, the accumulation layer shrank and $\langle n_{3D} \rangle$ eventually

increased to more than 1×10^{20} cm^{-3} (the carrier density giving the maximum T_c in chemically doped $SrTiO_3$ (ref. 6)). Here, we note that the subband structure was also substantially modified with increasing V_G owing to the increase of the confinement potential (see Supplementary Information, Fig. S3). Subband splitting energies were enhanced with increasing V_G, which virtually cancels out the increase in E_F, leading to a fairly constant DOS at E_F, as shown in the bottom panel of Fig. 4b. This picture is a unique and unexpected feature of the electronic state due to the incipient ferroelectricity of $SrTiO_3$, and could be related to the almost constant T_c of superconductivity. Achieving superconductivity in a clean ferroelectric medium will be an interesting challenge for physicists in terms of low-carrier-density superconductors with pure two-dimensionality and broken inversion symmetry.

References

1. Ahn, C. H. *et al.* Electrostatic modulation of superconductivity in ultrathin GdBa$_2$Cu$_3$O$_{7-x}$ films. *Science* **284**, 1152–1155 (1999).
2. Ahn, C. H., Triscone, J.-M. & Mannhart, J. Electric field effect in correlated oxide systems. *Nature* **424**, 1015–1018 (2003).
3. Takahashi, K. S. *et al.* Electrostatic modulation of the electronic properties of Nb-doped SrTiO$_3$ superconducting films. *Appl. Phys. Lett.* **84**, 1722–1724 (2004).
4. Takahashi, K. S. *et al.* Local switching of two-dimensional superconductivity using the ferroelectric field effect. *Nature* **441**, 195–198 (2006).
5. Kötz, R. & Carlen, M. Principles and applications of electrochemical capacitors. *Electrochim. Acta* **45**, 2483–2498 (2000).
6. Schooley, J. F. *et al.* Dependence of the superconducting transition temperature on carrier concentration in semiconducing SrTiO$_3$. *Phys. Rev. Lett.* **14**, 305–307 (1965).
7. Ohno, H. *et al.* Electric-field control of ferromagnetism. *Nature* **408**, 944–946 (2000).
8. Glover, R. E. & Sherrill, M. D. Changes in superconducting critical temperature produced by electrostatic charging. *Phys. Rev. Lett.* **5**, 248–250 (1960).
9. Ueno, K. *et al.* Field-effect transistor on SrTiO$_3$ with sputtered Al$_2$O$_3$ gate insulator. *Appl. Phys. Lett.* **83**, 1755–1757 (2003).
10. Shibuya, K. *et al.* Field-effect modulation of the transport properties of nondoped SrTiO$_3$. *Appl. Phys. Lett.* **88**, 212116 (2006).
11. Nakamura, H. *et al.* Low temperature metallic state induced by electrostatic carrier doping of SrTiO$_3$. *Appl. Phys. Lett.* **89**, 133504 (2006).
12. Sato, T., Shibuya, K., Ohnishi, T., Nishio, K. & Lippmaa, M. Fabrication of SrTiO$_3$ field effect transistors with SrTiO$_{3-\delta}$ source and drain electrodes. *Jpn. J. Appl. Phys.* **46**, L515–L518 (2007).
13. Dhoot, A. S. *et al.* Beyond the metal–insulator transition in polymer electrolyte gated polymer field-effect transistors. *Proc. Natl Acad. Sci* **103**, 11834–11837 (2006).
14. Panzer, M. J. & Frisbie, C. D. High carrier density and metallic conductivity in poly(3-hexylthiophene) achieved by electrostatic charge injection. *Adv. Funct. Mater.* **16**, 1051–1056 (2006).
15. Misra, R., McCarthy, M. & Hebard, A. F. Electric field gating with ionic liquids. *Appl. Phys. Lett.* **90**, 052905 (2007).
16. Shimotani, H. *et al.* Insulator-to-metal transition in ZnO by electric double layer gating. *Appl. Phys. Lett.* **91**, 082106 (2007).
17. Kawasaki, M. *et al.* Atomic control of the SrTiO$_3$ crystal surface. *Science* **266**, 1540–1542 (1994).
18. Tufte, O. N. & Chapman, P. W. Electron mobility in semiconducting strontium titanate. *Phys. Rev.* **155**, 796–802 (1967).
19. Shimotani, H., Asanuma, H., Takeya, J. & Iwasa, Y. Electrolyte-gated charge accumulation in organic single crystals. *Appl. Phys. Lett.* **89**, 203501 (2006).
20. Ohtomo, A. & Hwang, H. Y. A high-mobility electron gas at the LaAlO$_3$/SrTiO$_3$ heterointerface. *Nature* **427**, 423–426 (2004).
21. Brinkman, A. *et al.* Magnetic effects at the interface between non-magnetic oxides. *Nature Mater.* **6**, 493–496 (2007).
22. Reyren, N. *et al.* Superconducting interfaces between insulating oxides. *Science* **317**, 1196–1199 (2007).
23. Ando, T., Fowler, A. B. & Stern, F. Electronic properties of two-dimensional systems. *Rev. Mod. Phys.* **54**, 437–672 (1982).
24. Neville, R. C., Hoeneisen, B. & Mead, C. A. Permittivity of strontium titanate. *J. Appl. Phys.* **43**, 2124–2131 (1972).
25. Mattheiss, L. F. Energy bands for KNiF$_3$, SrTiO$_3$, KMoO$_3$, and KTaO$_3$. *Phys. Rev. B.* **6**, 4718–4740 (1972).
26. Uwe, H., Yoshizaki, R., Sakudo, T., Izumi, A. & Uzumaki, T. Conduction band structure of SrTiO$_3$. *Jpn. J. Appl. Phys.* **24** (suppl. 24-2), 335–337 (1985).
27. Frederikse, H. P. R., Hosler, W. R., Thurber, W. R., Babiskin, J. & Siebenmann, P. G. Shubnikov–de Haas effect in SrTiO$_3$. *Phys. Rev.* **158**, 775–778 (1967).
28. Herranz, G. *et al.* Full oxide heterostructure combining a high-T_C diluted ferromagnet with a high-mobility conductor. *Phys. Rev. B* **73**, 64403 (2006).

Supplementary Information accompanies the paper at www.nature.com/naturematerials.

Author information
Reprints and permissions information is available online at http://npg.nature.com/reprintsandpermissions. Correspondence and requests for materials should be addressed to K.U. or M.K.